

Kinesin's second step

Lisa M. Klump^{*†}, Andreas Hoenger[‡], and Susan P. Gilbert^{*§}

^{*}Department of Biological Sciences, University of Pittsburgh, Pittsburgh, PA 15260; and [‡]European Molecular Biology Laboratory, Meyerhofstrasse 1, D-69012 Heidelberg, Germany

Edited by Thomas D. Pollard, Yale University, New Haven, CT, and approved January 21, 2004 (received for review November 21, 2003)

We have identified dimeric kinesin mutants that become stalled on the microtubule after one ATP turnover, unable to bind and hydrolyze ATP at their second site. We have used these mutants to determine the regulatory signal that allows ATP to bind to the forward head, such that processive movement can continue. The results show that phosphate release occurs from the rearward head before detachment, and detachment triggers active-site accessibility for ATP binding at the forward head. This mechanism, in which the rearward head controls the behavior of the forward head, may be conserved among processive motors.

Conventional kinesin is a plus-end-directed microtubule (Mt) motor protein that carries membranous organelles toward the synapse in neurons. Kinesin moves processively by coordinating its two motor domains, taking many steps along the Mt for distances of up to 1 μm before detaching (1–3). The ATPase cycle of kinesin allows for strict coordination of the motor domains, such that at least one motor domain of the dimer is bound tightly to the Mt during translocation (4–11). The ATPase mechanism of kinesin has been defined, although the focus has been on understanding kinesin's first step, which is coupled to one ATP turnover (Fig. 1).

Movement begins as kinesin binds the Mt with rapid release of ADP, forming Species 1 (Fig. 1). One head is bound to the Mt and is nucleotide-free, whereas the other head is tethered with ADP at its active site (5, 7, 9). ATP binds rapidly to the nucleotide-free, Mt-bound head. ATP binding leads to a series of structural transitions (5, 8–10, 12–21), one of which is believed to dock the neck linker onto the catalytic core, as reported by Rice *et al.* (15). The energy of ATP binding, coupled to neck-linker docking, leads to the plus-end-directed forward swing of the partner motor domain toward the next Mt-binding site (Species 3) (10, 12, 13, 15, 16). This head collides with the Mt in a weakly bound state, releasing its ADP (Species 4) (5, 9). ATP hydrolysis on the rearward head results in the forward head becoming tightly bound to the Mt (22, 23). Both heads are now tightly bound to the Mt (Species 5), which is believed to generate strain (10, 24). The strain is relieved by detachment of the rearward head, and the cycle begins again. An important component of the alternating-site mechanism was the observation that ATP binding is delayed on the forward head, although ADP is absent from its active site (5, 9, 10, 25). It has been proposed (24) that internal strain prevents ATP binding at the forward head. In addition, another important discovery was the recent observation that Mt binding closes the nucleotide pocket of kinesin, leading to domain movements of switch 1 for Mt-activated ATP hydrolysis (14).

Key questions remain for understanding kinesin mechanochemistry, including the elucidation of the regulatory signal that allows ATP binding at forward head and definition of the nucleotide state (ADP·P_i or ADP) of the rearward head that detaches from the Mt. For the dimeric wild-type motor wild-type construct comprising the N-terminal 401 amino acids of *Drosophila melanogaster* kinesin (K401), it was shown that phosphate release was coupled to dissociation from the Mt, with one step occurring at a fast rate and the other at a slow rate (4). Because only the slower rate constant can be detected, it has remained unclear whether kinesin detaches from the Mt before phosphate release or whether phosphate release occurs first from the

Mt-bound motor, followed by detachment of the K·ADP intermediate. Furthermore, it is possible that detachment from the Mt or phosphate release from head 1 is the signal that permits ATP binding and hydrolysis on head 2 for kinesin's second step (Fig. 1, Species 8).

We have identified two *D. melanogaster* kinesin mutants, K401-E164A and K401-E164K, which have allowed us to address these questions (26, 27). Both mutants are dimeric motors, yet both mutants become stalled on the Mt after one ATP turnover (Fig. 1, Species 5 or 6). We have used these mutants to determine whether phosphate release triggers the structural transitions for ATP to bind to the forward head or whether rearward-head detachment is the regulatory signal. The results presented show that phosphate release occurs first from the rearward head before detachment and that detachment is the signal triggering active-site accessibility for ATP binding at the forward head.

Materials and Methods

Materials. Bacterial purine nucleoside phosphorylase (PNPase) and 7-methylguanosine (MEG) were purchased from Sigma, and *N*-[2-(1-maleimidyl)ethyl]-7-(diethylamino)coumarin-3-carboxamide (MDCC) was purchased from Molecular Probes. The phosphate-binding protein (PBP) used to generate the MDCC-PBP probe contains an A197C mutation, and cysteine residue 197 was modified with the MDCC (28). The pSN5182 plasmid containing the A197C substitution and the fluorescent PBP-coupled assay were developed by Martin R. Webb and colleagues (National Institute of Medical Research, Mill Hill, London) and are described in detail in ref. 28.

Kinesin Motors. The kinesin mutants E164A and E164K were constructed by introducing a single amino acid change in the wild-type K401 plasmid pET5b-K01, as described (26, 27). The proteins were expressed in *Escherichia coli* BL21(DE3)pLysS and purified to >95% homogeneity, as described (26, 27). Reported motor concentrations represent single-motor domains (or ATP-binding sites), although E164A and E164K are both dimeric. E164A and E164K were purified with ADP tightly bound at the active site (data not shown).

Experimental Conditions. All experiments reported were performed in ATPase buffer containing 20 mM Hepes-KOH (pH 7.2), 5 mM magnesium acetate, 0.1 mM EGTA, 0.1 mM EDTA, 50 mM potassium acetate, and 1 mM DTT at 25°C. The concentrations reported are the final concentrations after mixing, unless indicated otherwise.

This paper was submitted directly (Track II) to the PNAS office.

Abbreviations: K401/341, construct comprising the N-terminal 401/341 amino acids of *Drosophila melanogaster*; Mt, microtubule; mantATP/ADP, 2'(3')-O-(*N*-methylanthraniloyl)-ATP/ADP; PBP, phosphate-binding protein; MDCC, *N*-[2-(1-maleimidyl)ethyl]-7-(diethylamino)coumarin-3-carboxamide; MEG, 7-methylguanosine; PNPase, bacterial purine nucleoside phosphorylase.

[†]Present address: Department of Pharmacology, University of Pennsylvania School of Medicine, 131 John Morgan Building, 3610 Hamilton Walk, Philadelphia, PA 19104-6084.

[§]To whom correspondence should be addressed at: Department of Biological Sciences, 518 Langley Hall, University of Pittsburgh, Pittsburgh, PA 15260. E-mail: spg1@pitt.edu.

© 2004 by The National Academy of Sciences of the USA

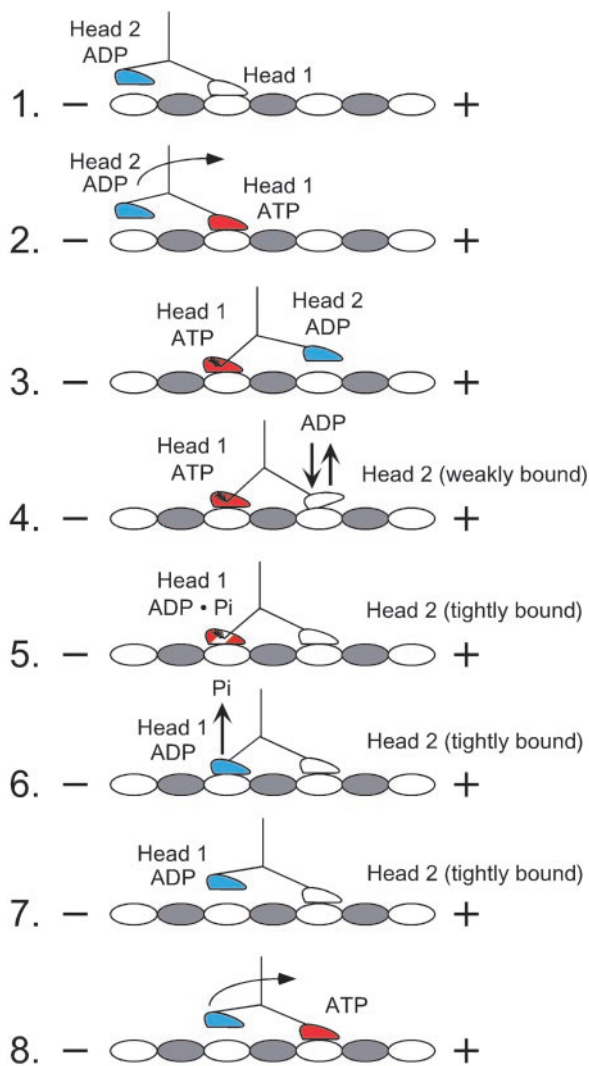


Fig. 1. Walking model defining kinesin's second step. Head 1 binds the Mt with rapid ADP release. ATP binding at head 1 leads to the plus-end-directed motion of the neck linker to position head 2 forward at the next Mt-binding site. ATP binding at head 1 promotes head 2 binding to the Mt, followed by rapid ADP release. ATP hydrolysis at head 1 locks head 2 onto the Mt in a tight-binding state. Phosphate release occurs on head 1, followed by detachment from the Mt. The active site of head 2 is then accessible for ATP binding, and the cycle is repeated.

Pre-Steady-State Kinetics. Dissociation of the Mt-kinesin complex (Fig. 2E) was determined by the change in light scattering, monitored at 320 nm. Each transient was normalized to begin at 6 V for direct comparison of transient amplitudes. The kinetics of 2'(3')-O-(N-methylanthraniloyl)-ATP (mantATP) binding (Fig. 2F–H) were measured in the stopped-flow instrument with excitation at 360 nm, and fluorescence emission was detected at 450 nm by using a 400-nm cutoff filter. The transients were normalized to begin at 6.0 V.

Phosphate-Release Kinetics. The kinetics of phosphate release were measured by using a coupled-assay system with MDCC-PBP, as described (4, 28). The MDCC fluorophore was excited at 425 nm with fluorescence emission detected at 474 nm by using a 450-nm cutoff filter. To remove free phosphate from the solutions and the stopped-flow observation cell, a “P_i Mop,” consisting of 0.15 mM MEG plus 0.05 units/ml PNPase was used to sequester contaminating free phosphate as ribose-1-

phosphate. The concentrations of MEG and PNPase were adjusted to achieve a rate of phosphate removal at 0.005 s⁻¹. At these conditions, the “Mop reaction” did not compete with the MDCC-PBP for P_i. In the stopped flow, the reactants in Syringe A were rapidly mixed with reactants of Syringe B. Syringe concentrations of reactants were as follows: Syringe A, Mt-motor complex (1 μM motor; Mts at 2 μM tubulin/20 μM taxol), 10 μM MDCC-PBP, 0.15 mM MEG, and 0.05 units/ml PNPase in ATPase buffer; and Syringe B, varying MgATP (1.5 μM to 2 mM), 200 mM potassium chloride (in addition to 50 mM potassium acetate of the buffer), 0.15 mM MEG, and 0.05 units/ml PNPase in ATPase buffer. This experimental design resulted in final concentrations after mixing of 0.5 μM motor, 1 μM Mts, 10 μM taxol, 5 μM MDCC-PBP, varying MgATP, 100 mM potassium chloride, 0.15 mM MEG, and 0.05 units/ml PNPase in ATPase buffer, with final salt concentration contributed by potassium acetate plus potassium chloride at 150 mM. For kinesin, low concentrations of Mts and added salt are traditionally used to slow subsequent turnovers of ATP so that the burst rate and amplitude of the first ATP turnover can be well defined (4, 6).

To convert the PBP amplitude data from volts into units of concentration (which can be related to enzyme concentration), a phosphate standard curve was used. Syringe concentrations of reactants were as follows. Syringe A, containing 10 μM MDCC-PBP, 0.05 units/ml PNPase, and 0.15 mM MEG in ATPase buffer, reacted with Syringe B, containing varying amounts of KH₂PO₄ in ddH₂O, to avoid any free phosphate contamination. Final concentrations were as follows: 5 μM MDCC-PBP/0.025 units/ml PNPase/0.075 mM MEG/varying KH₂PO₄/ATPase buffer components at one-half of the original concentration. Transients at these lower salt concentrations were equivalent to transients at 150 mM salt (data not shown). The amplitude of each transient was determined in volts and plotted as a function of phosphate concentration. The linear fit was used to convert the amplitude of the experimental transients in volts to μM P_i, based on the phosphate-calibration curve.

To ensure that the initial amplitude of the stopped-flow signal was not lost in the dead-time of the instrument, the instrument was set to show the data during the first 1.4–2 ms of mixing. Also, this experimental design facilitated the normalization of the transients such that all would begin at the same point on the y axis. All experiments shown within a single species (1–8) in Fig. 2 were performed on the same day with the same stock solutions and single setting of the high-voltage sensitivity of the stopped-flow instrument to avoid variability introduced by different Mt, motor, ATP, mantATP, and salt/buffer solutions. The stopped-flow transients represent the mean of 5–12 individual records.

Results

The E164A mutant binds ATP and Mts with a higher affinity than wild-type kinesin, and the dimeric mutant becomes stalled on the Mt after ATP hydrolysis and, thus, unable to detach from the Mt or bind ATP to the partner motor domain (27). This mutant was used to determine whether phosphate release occurred from the Mt-bound intermediate before detachment (Fig. 1, Species 5) or whether detachment from the Mt was a prerequisite for phosphate release from the active site of the motor. The pre-steady-state kinetics of phosphate release were measured directly by using the MDCC-PBP fluorescence assay developed by Martin R. Webb and coworkers (28). The Mt·E164A complex was preformed (Fig. 1, Species 1) and rapidly mixed with MgATP plus potassium chloride. Fig. 2A *Inset* shows a representative transient at 300 μM MgATP (final concentrations 0.5 μM E164A, 1 μM Mts, 300 μM MgATP, and 150 mM salt). The Mt-kinesin complex binds and hydrolyzes ATP. The P_i, when released from the active site of the motor, is bound rapidly and tightly by MDCC-PBP, leading to the observed exponential

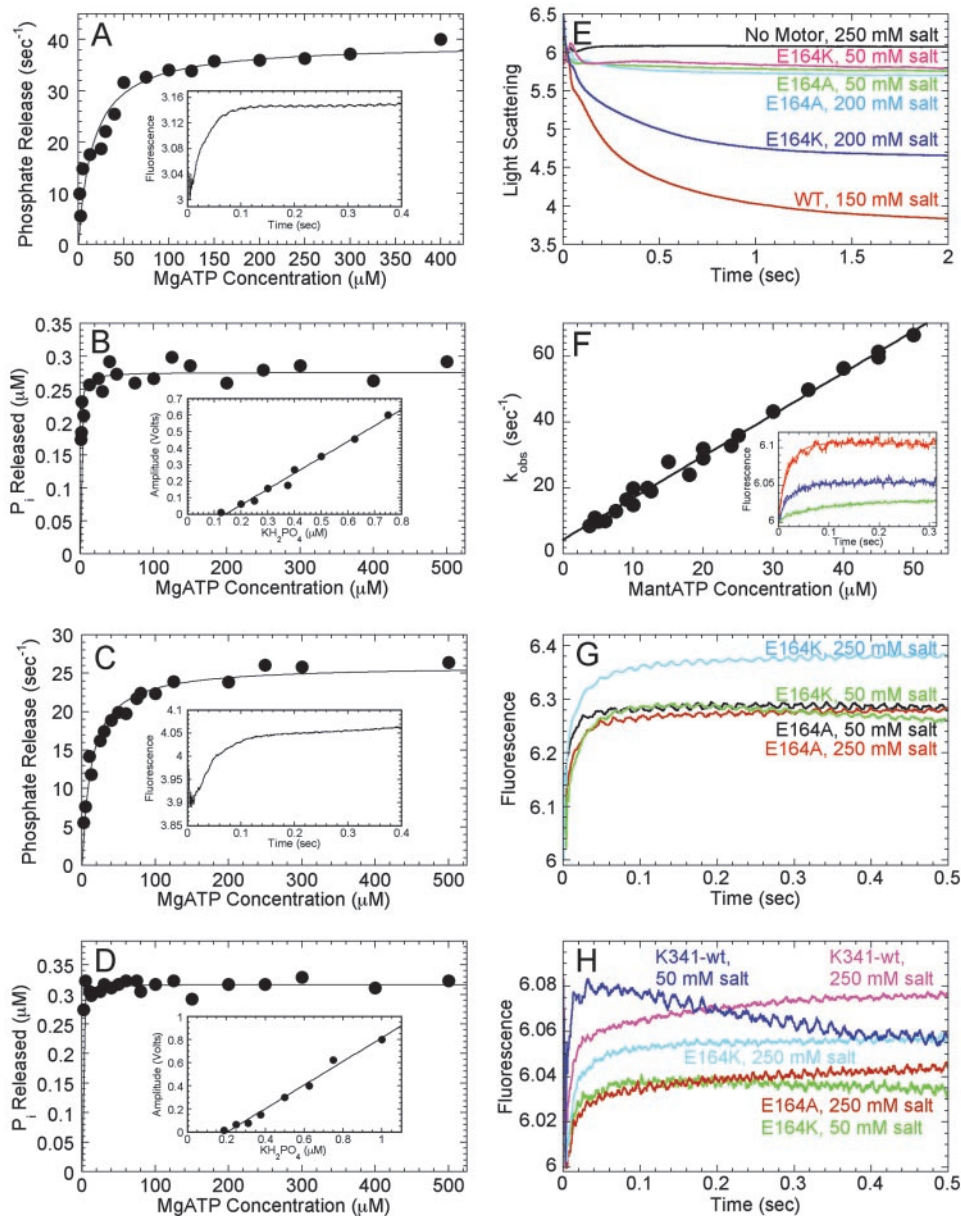


Fig. 2. Pre-steady-state kinetics of E164A and E164K. (A and B) The Mt-E164A complex plus MDCC-PBP was mixed with various concentrations of MgATP plus potassium chloride. Final concentrations are as follows: 0.5 μM E164A, 1 μM tubulin, 10 μM taxol, 5 μM MDCC-PBP, 0.05 units/ml PNPase, 0.15 mM MEG, MgATP, and 100 mM potassium chloride (in addition to 50 mM potassium acetate in the buffer). *A Inset* shows a representative transient of the Mt-E164A complex at 300 μM MgATP ($k_{\text{obs}} = 37.2 \pm 0.2 \text{ s}^{-1}$, relative amplitude = 0.138 ± 0.0008 V). The rate of the exponential fluorescence enhancement increases as a function of MgATP. The fit of the data to a hyperbola provides the maximum-rate constant for phosphate release for E164A at 150 mM salt, $k_{\text{obs}} = 39.1 \pm 1.6 \text{ s}^{-1}$; $K_{1/2, \text{ATP}} = 16.6 \pm 3.2 \text{ μM}$. (B) Amplitudes of each of the phosphate transients in units of concentration were plotted as a function of ATP concentration. The fit of the data to a hyperbola provided the maximum amplitude $0.275 \pm 0.0045 \text{ μM P}_i$, which corresponds to 55.0 ± 0.9% of the 0.5 μM E164A sites. *Inset* shows the calibration curve used to convert the burst amplitude in volts to sites binding P_i. (C and D) Phosphate-release kinetics for E164K. Conditions are as described for A. *C Inset* shows the phosphate-release kinetics for the Mt-E164K complex at 300 μM MgATP ($k_{\text{obs}} = 25.8 \pm 0.2 \text{ s}^{-1}$, relative amplitude = 0.131 ± 0.0009 V). The observed rate of the initial exponential fluorescence enhancement of each transient was plotted as a function of MgATP concentration. The maximum-rate constant for phosphate release for E164K at 150 mM salt, $k_{\text{obs}} = 26.0 \pm 0.57 \text{ s}^{-1}$; $K_{1/2, \text{ATP}} = 13.1 \pm 1.4 \text{ μM}$. (D) Amplitude in volts of each E164K phosphate transient was converted to units of concentration by using the calibration curve shown in *Inset*. The maximum amplitude at $0.32 \pm 0.0029 \text{ μM P}_i$ corresponds to 64.0 ± 0.6% of the 0.5 μM E164K sites. (E) ATP-promoted dissociation of the Mt-kinesin complex. The preformed Mt-motor complex was mixed with 2 mM MgATP in ATPase buffer with 50 mM potassium acetate plus additional potassium chloride. Final concentrations are as follows: 3 μM motor, 2.9 μM tubulin, 20 μM taxol, 1 mM MgATP, and various concentrations of salt. (F–H) MantATP-binding kinetics. (F) A preformed Mt-E164K complex was rapidly mixed in the stopped-flow instrument with varying concentrations of mantATP in ATPase buffer containing (final concentrations) 3 μM motor, 10 μM tubulin, 20 μM taxol, varying concentrations of mantATP, and 50 mM potassium acetate from buffer. Representative transients, shown from the top to the bottom transient, are 40, 25, and 6 μM mantATP, with the fit of the data to a single exponential function, shown by the smooth line. The rate of the exponential fluorescence enhancement was plotted as a function of mantATP concentration, and the slope provides the second-order rate constant $k_{\text{on}} = 1.26 \pm 0.03 \text{ μM}^{-1} \text{ s}^{-1}$. (G) MantATP-binding kinetics at 20 μM mantATP to compare relative amplitudes. Final concentrations are as follows: 5 μM motor, 15 μM tubulin, 20 μM taxol, and 20 μM mantATP. The final salt concentration includes the contribution of 50 mM potassium acetate present in the buffer. (H) MantATP-binding kinetics at 100 μM mantATP to compare the relative amplitudes of dimeric E164A and E164K with monomeric kinesin, wild-type K341. Final concentrations are as follows: 5 μM motor, 15 μM tubulin, 20 μM taxol, 100 μM mantATP, and 50 or 250 mM salt.

increase in fluorescence (Fig. 2*A Inset*). The observed rate of the fluorescence enhancement, associated with phosphate release from E164A, increased as a function of ATP concentration. The results show that the maximum-rate constant for phosphate release from E164A was rapid at 40 s^{-1} (Fig. 2*A*). Experiments (data not shown) were also performed in which the Mt·E164A complex was preformed with Mt-binding sites at a 5-fold excess of motor-domain concentration ($1 \mu\text{M}$ E164A plus $5 \mu\text{M}$ Mts), to exclude concerns about motor crowding, as well as at higher concentrations ($5 \mu\text{M}$ E164A plus $10 \mu\text{M}$ Mt), to determine whether the rate constant observed for phosphate release was limited by the concentration of P_i released from the motor during the first ATP turnover. The phosphate-release kinetics at these other conditions did not vary significantly from the data presented in Fig. 2. Because E164A does not detach from the Mt (27), the kinetics document that detachment is not a required structural transition for phosphate release from the rearward head.

When this experiment was performed for wild-type K401, the phosphate-release kinetics were biphasic and the rate observed for the initial exponential phase was 13 s^{-1} (4). The intrinsic rate constant for phosphate release from each head of wild-type K401 was modeled at 50 s^{-1} (5, 6, 11), which is consistent with the observed rate for a dimeric processive motor that shows an alternating-site ATPase mechanism for stepping. Only one head of the kinesin dimer is active at a given time, therefore, the observed rate represents the net rate of phosphate release from both heads for multiple ATP turnovers. Note that the phosphate-release kinetics for E164A (Fig. 2*A Inset*) are not biphasic and fit a single exponential function, suggesting that the kinetics represent phosphate release from one active site. The observation that phosphate release for E164A occurs at 40 s^{-1} suggests that we have measured phosphate release that results from the first ATP turnover on head 1 (Fig. 1, Species 1–6). In addition, phosphate release was observed from the E164A mutant, which does not dissociate from the Mt, indicating that phosphate release occurs from the Mt-bound intermediate and, therefore, K·ADP is the intermediate that detaches from the Mt (Fig. 1, Species 7).

To determine whether the phosphate-release kinetics in Fig. 2*A* represented one or both active sites of the E164A dimer, a standard curve was generated to convert the fluorescence amplitude from volts into μM P_i (Fig. 2*B*). Phosphate release was saturated with an amplitude of $0.27 \mu\text{M}$, which corresponds to 55% of the $0.5 \mu\text{M}$ E164A sites in this experiment. We have measured the phosphate-release kinetics for E164A on various days and at saturating ATP concentrations (250 – $1,000 \mu\text{M}$) by using three preparations of E164A and two preparations of MDCC-PBP. The amplitude associated with phosphate release for these individual transients showed a range of 34.0–59.6% of active sites, with $48.2 \pm 1.7\%$ (mean \pm SEM; $n = 19$). These data are consistent with the interpretation that phosphate release is occurring from head 1 after one ATP turnover (Fig. 1, Species 6).

We proposed (27), based on acid-quench and pulse-chase kinetics, that only one of the two catalytic motor domains of E164A can bind and hydrolyze ATP. Thus, the E164A mutant is competent to bind ATP, hydrolyze ATP, and release phosphate from head 1; however, the structural transitions that allow ATP binding and hydrolysis on head 2 are prevented. Based on the phosphate-release kinetics, we propose that detachment of the rearward head from the Mt is the structural transition, or trigger, that allows ATP to bind the forward motor domain.

The E164K mutant displays steady-state kinetics similar to E164A. For E164K, the $k_{\text{cat}} = 6.8 \pm 0.6 \text{ s}^{-1}$, $K_{\text{m,ATP}} = 21.3 \pm 2.8 \mu\text{M}$, and $K_{0.5,\text{Mt}} = 0.4 \pm 0.2 \mu\text{M}$. In comparison, the steady-state parameters for E164A are as follows: $k_{\text{cat}} = 4.9 \pm 0.5 \text{ s}^{-1}$, $K_{\text{m,ATP}} = 21.1 \pm 2.6 \mu\text{M}$, and $K_{0.5,\text{Mt}} = 0.4 \pm 0.1 \mu\text{M}$ (26, 27). For E164A, we proposed that the stalling on the Mt may occur

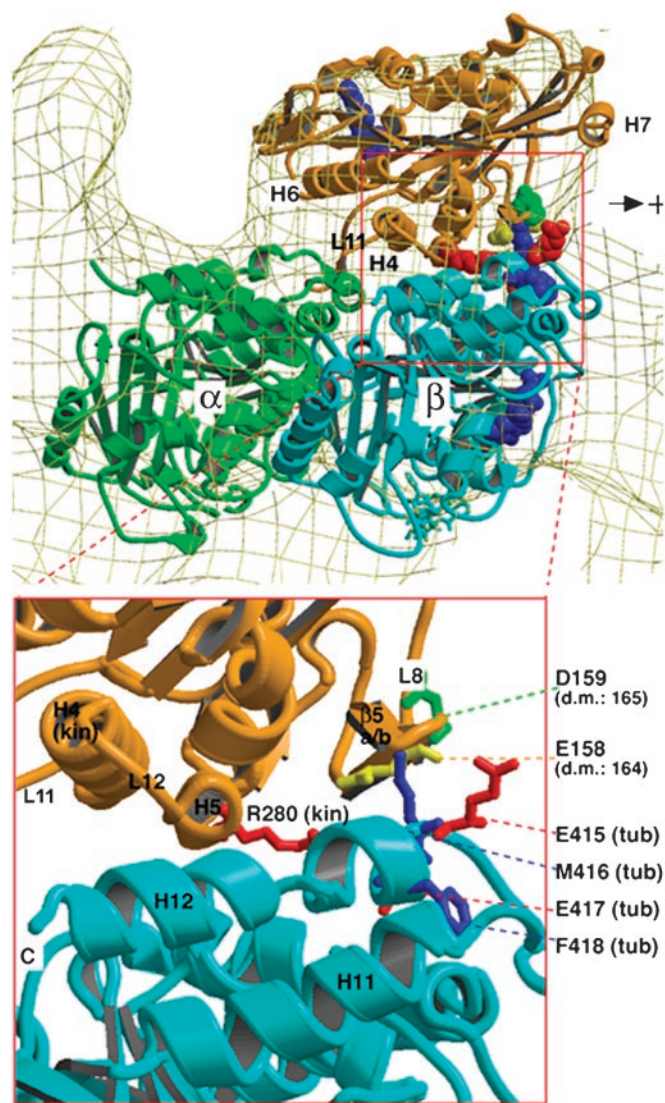


Fig. 3. Potential interactions of *Drosophila* E164 (rat E158) at the β -sheet 5a-loop 8b junction with Mt amino acids were determined by docking the monomeric rat kinesin 2KIN (33) into the cryo-EM 3D scaffold of a Mt-kinesin complex by using the atomic coordinates of α , β -tubulin (34) and the software package o (35). The kinesin motor domain is shown in yellow, and the amino acid residues are designated by the rat sequence (rat E158, D159; *D. melanogaster* E164, D165; and human E157, D158). The β -tubulin subunit (cyan) is shown nucleotide-bound (blue) and taxol-bound (cyan), and the Mt plus-end is shown to the right. The nucleotide-bound α -tubulin subunit is shown in green. Kinesin and the Mt interact predominantly through the C-terminal tubulin helices 12 and 11 (cyan). Note the close proximity of kinesin E158 to kinesin residue R280 on α -helix 5 and to β -tubulin residues E415, E417, M416, and F418 on α -helix 12. The key kinesin structural elements for Mt binding are the switch II cluster α 4-L12- α 5, loops L11 and L8, and β 5a,b. Kinesin α -helices 4, 5, 6, and 7 are designated H4, H5, H6, and H7, respectively.

because of stabilizing hydrophobic interactions with Met-416 and Phe-418 of β -tubulin α -helix 12 (Fig. 3). We reasoned that for E164K, the Mt-motor interface may be stabilized also but by means of electrostatic interactions between the E164K lysine side chain and Glu-415 and Glu-417 of β -tubulin α -helix 12. We assumed then that these electrostatic interactions could be disrupted with added salt. We predicted that adding salt plus ATP would lead to E164K dissociation from the Mt (Fig. 1, Species 7), yet E164A would remain associated with the Mt (Fig. 1, Species 6) because of the stabilizing hydrophobic interactions.

Fig. 2E presents the dissociation kinetics for E164K, E164A, and wild-type K401. The Mt-motor complex is preformed (Fig. 1, Species 1) and mixed rapidly in the stopped-flow instrument with MgATP plus salt. Wild-type kinesin at 150 mM salt displays a large decrease in light scattering that correlates with the motors detaching from the Mt. E164A does not detach with added ATP plus 200 mM salt, whereas E164K shows $\approx 60\%$ detachment at these conditions. These results are consistent with the interpretation that ATP can promote motor detachment of wild-type K401 and E164K, yet E164A appears to remain as a stable complex with the Mt, as shown (27).

Fig. 2C and D show the phosphate-release kinetics for E164K and also at 150 mM salt. Note that phosphate release occurs at 26 s^{-1} , an observed rate intermediate between that of wild-type K401 (13 s^{-1}) and E164A (40 s^{-1}). The amplitude data for the phosphate-release kinetics are presented in Fig. 2D. The burst amplitude at $0.31\text{ }\mu\text{M}$ for $0.5\text{ }\mu\text{M}$ E164K represents 62% of sites. When this experiment was repeated on different days at saturating ATP concentrations and with different protein preparations of E164K and MDCC-PBP, the individual transients of 16 experiments show a range in amplitude of 58.0–74.4% sites with $64 \pm 0.9\%$ sites (mean \pm SEM). Our interpretation is that, for E164K at 150 mM salt, we are beginning to see a population with detachment of head 1 (Fig. 1, Species 7), resulting in the ability of these kinesin motors to bind and hydrolyze ATP at head 2 (Fig. 1, Species 8) as well as at head 1 (Fig. 1, Species 2). For E164K, therefore, ATP binding, ATP hydrolysis, and phosphate release can occur from both head 1 and head 2. The intermediate-rate constant at 26 s^{-1} supports this interpretation as well.

One prediction of this hypothesis is that the Mt-E164K complex (Fig. 1, Species 1) at low salt conditions should bind ATP to head 1 only (Fig. 1, Species 2–4). Fig. 2F shows the mantATP-binding kinetics for E164K at 50 mM salt and as a function of mantATP concentration. The kinetics of the individual transients fit a single exponential function as expected if the kinetics represent mantATP binding to head 1 only. Yet, with additional salt to dissociate head 1 after ATP binding and hydrolysis, the active site at head 2 should become accessible for ATP binding (Fig. 1, Species 8). Fig. 2G shows the mantATP-binding kinetics for the Mt-E164K complex and the Mt-E164A complex, with final salt concentrations of 50 mM and 250 mM. The mantATP-binding transients for E164A at 50 mM and 250 mM salt, as well as E164K at 50 mM salt, are very similar, and the amplitudes of each transient are the same. In contrast, for E164K at 250 mM salt, there is a significant increase in the amplitude associated with mantATP binding. Our interpretation of these data are that the transients for E164A and E164K at low salt represent mantATP binding at head 1 of the dimer (Fig. 1, Species 1–4). However, the E164K transient at 250 mM salt represents a population of dimers that show mantATP binding to both head 1 and head 2 (Species 1–8). If we assume that the E164A transients represent 50% of the sites binding ATP, then the E164K transient at 250 mM salt would represent 70% of the sites.

The experiments shown in Fig. 2G provide qualitative amplitude data that supported our interpretation, but we designed another experiment that would be more definitive (Fig. 2H). First, we used a kinesin monomer, a wild-type construct comprising the N-terminal 341 amino acids of *D. melanogaster* kinesin (K341), to show the fluorescence amplitude for 100% occupancy by mantATP. Second, we increased the mantATP concentration to $100\text{ }\mu\text{M}$ to ensure that all motor sites would be saturated with mantATP. The wild-type K341 transient at 50 mM salt (Fig. 2, blue) shows the biphasic kinetics characteristic of monomeric kinesin (6, 8). This experiment was repeated with additional salt included in the mantATP syringe (Fig. 2, fuchsia). At 250 mM salt, wild-type K341 dissociates from the Mt;

therefore, all active sites should be occupied by mantADP by 0.5 s. mantADP and mantATP provide similar fluorescence enhancement for wild-type K341 (data not shown); therefore, the wild-type K341 experiments at $100\text{ }\mu\text{M}$ mantATP provide the fluorescence amplitude expected for 100% occupancy of the active sites. E164K at 50 mM salt and E164A at 250 mM salt show the same relative amplitudes, indicating 50% occupancy by mantATP. The amplitude of the E164K transient at 250 mM salt is significantly higher than E164K at 50 mM salt. Its relative amplitude at 0.055 ± 0.0007 indicates 70.5% occupancy.

These results support the hypothesis that detachment of head 1 is the mechanistic signal for the second motor domain to bind and hydrolyze ATP for forward movement.

Discussion

Kinesin's first step (Fig. 1, Species 1–5) has been well defined by examining the conformational and mechanistic changes that occur as the first head collides with the Mt and binds ATP. However, until now, kinesin's second step has not been defined. Moreover, the gate that prevents ATP from prematurely binding to head 2 has been elusive. The proposal that ATP binding was delayed on the forward head until the rearward head detached could not be rigorously tested previously because detachment and phosphate release were coupled in the wild-type motor (4, 9, 10, 25). Moreover, it was predicted that internal strain generated when both motor domains are bound to the Mt prevents ATP binding at the leading head (24). Our kinesin mutants have allowed us to dissect the order of events that allow ATP binding on the forward head for processive movement.

Here we present evidence that phosphate release can occur from the Mt-K \cdot ADP-P_i intermediate (Fig. 1, Species 5) and have measured the rate of phosphate release at 40 s^{-1} from the E164A motor, similar to the intrinsic-rate constant modeled for wild-type kinesin at 50 s^{-1} . The E164A mutant has uncoupled phosphate release from Mt detachment and has allowed us to define kinesin's second step further. We propose that detachment of head 1 (Species 7) is the mechanistic signal that allows ATP binding and hydrolysis on the second motor domain. These results also indicate that phosphate release is the rate-limiting step of the wild-type Mt-kinesin ATPase pathway with rearward-head detachment occurring rapidly when phosphate is released from the active site.

These data also support the idea that the rearward head (head 1) controls the next event in the forward head (head 2). This observation has broader implications for the way that dimeric motor proteins communicate with their partner motor domains to achieve the elegant cooperative interactions necessary for processive movement. For myosin VI, De La Cruz *et al.* (29) proposed that the forward head cannot bind F-actin strongly because it is restrained by the trailing head, suggesting also that the backward head controls the forward head. However, this mechanism is not yet well established for the processive myosins V and VI (see refs. 30 and 31). In addition, our results are inconsistent with the inchworm model, as proposed by Hua *et al.* (32) because, in this model, only one ATP is hydrolyzed per dimer and the forward motor domain would dictate the action of the rearward head because the forward head always leads. In summary, the *Drosophila* Glu-164 alanine and lysine mutants have allowed us to order the events that define kinesin's second step and to propose a mechanism that may be a common strategy for processive motors.

We thank Dr. Martin R. Webb (National Institute for Medical Research, Mill Hill, London) for the PBP clone and help in developing the assay in our laboratory and Jared C. Cochran (University of Pittsburgh) for help with the experiment shown in Fig. 2H. This work was supported by National Institute of General Medical Sciences Grant GM54141 and National Institute of Arthritis and Musculoskeletal and Skin Diseases Career Development Award K02-AR47841 (to S.P.G.).

1. Vale, R. D. & Milligan, R. A. (2000) *Science* **288**, 88–95.
2. Schief, W. R. & Howard, J. (2001) *Curr. Opin. Cell Biol.* **13**, 19–28.
3. Schliwa, M. & Woehlke, G. (2003) *Nature* **422**, 759–765.
4. Gilbert, S. P., Webb, M. R., Brune, M. & Johnson, K. A. (1995) *Nature* **373**, 671–676.
5. Gilbert, S. P., Moyer, M. L. & Johnson, K. A. (1998) *Biochemistry* **37**, 792–799.
6. Moyer, M. L., Gilbert, S. P. & Johnson, K. A. (1998) *Biochemistry* **37**, 800–813.
7. Hackney, D. D. (1994) *Proc. Natl. Acad. Sci. USA* **91**, 6865–6869.
8. Ma, Y.-Z. & Taylor, E. W. (1995) *Biochemistry* **34**, 13242–13251.
9. Ma, Y.-Z. & Taylor, E. W. (1997) *J. Biol. Chem.* **272**, 724–730.
10. Rosenfeld, S. S., Xing, J., Jefferson, G. M., Cheung, H. C. & King, P. H. (2002) *J. Biol. Chem.* **277**, 36731–36739.
11. Mandelkow, E. & Johnson, K. A. (1998) *Trends Biochem. Sci.* **23**, 429–433.
12. Schnitzer, M. J., Visscher, K. & Block, S. M. (2000) *Nat. Cell Biol.* **2**, 718–723.
13. Skiniotis, G., Surrey, T., Altmann, S., Gross, H., Song, Y. H., Mandelkow, E. & Hoenger, A. (2003) *EMBO J.* **22**, 1518–1528.
14. Naber, N., Minehardt, T. J., Rice, S., Chen, X., Grammer, J., Matuska, M., Vale, R. D., Kollman, P. A., Car, R., Yount, R. G., *et al.* (2003) *Science* **300**, 798–801.
15. Rice, S., Lin, A. W., Safer, D., Hart, C. L., Naber, N., Carragher, B. O., Cain, S. M., Pechatnikova, E., Wilson-Kubalek, E. M., Whittaker, M., *et al.* (1999) *Nature* **402**, 778–784.
16. Rice, S., Cui, Y., Sindelar, C., Naber, N., Matuska, M., Vale, R. & Cooke, R. (2003) *Biophys. J.* **84**, 1844–1854.
17. Sindelar, C. V., Budny, M. J., Rice, S., Naber, N., Fletterick, R. & Cooke, R. (2002) *Nat. Struct. Biol.* **9**, 844–848.
18. Gilbert, S. P. & Johnson, K. A. (1994) *Biochemistry* **33**, 1951–1960.
19. Rosenfeld, S. S., Jefferson, G. M. & King, P. H. (2001) *J. Biol. Chem.* **276**, 40167–40174.
20. Xing, J., Wriggers, W., Jefferson, G. M., Stein, R., Cheung, H. C. & Rosenfeld, S. S. (2000) *J. Biol. Chem.* **275**, 35413–35423.
21. Asenjo, A. B., Krohn, N. & Sosa, H. (2003) *Nat. Struct. Biol.* **10**, 836–842.
22. Farrell, C. M., Mackey, A. T., Klumpp, L. M. & Gilbert, S. P. (2002) *J. Biol. Chem.* **277**, 17079–17087.
23. Klumpp, L. M., Mackey, A. T., Farrell, C. M., Rosenberg, J. M. & Gilbert, S. P. (2003) *J. Biol. Chem.* **278**, 39059–39067.
24. Rosenfeld, S. S., Fordyce, P. M., Jefferson, G. M., King, P. H. & Block, S. M. (2003) *J. Biol. Chem.* **278**, 18550–18556.
25. Hackney, D. D. (2002) *Biochemistry* **41**, 4437–4446.
26. Brendza, K. M., Rose, D. J., Gilbert, S. P. & Saxton, W. M. (1999) *J. Biol. Chem.* **274**, 31506–31514.
27. Klumpp, L. M., Brendza, K. M., Rosenberg, J. M., Hoenger, A. & Gilbert, S. P. (2003) *Biochemistry* **42**, 2595–2606.
28. Brune, M., Hunter, J. L., Corrie, J. E. T. & Webb, M. R. (1994) *Biochemistry* **33**, 8262–8271.
29. De La Cruz, E. M., Ostap, E. M. & Sweeney, H. L. (2001) *J. Biol. Chem.* **276**, 32373–32381.
30. Veigel, C., Wang, F., Bartoo, M. L., Sellers, J. R. & Molloy, J. E. (2002) *Nat. Cell Biol.* **4**, 59–65.
31. Tyska, M. J. & Mooseker, M. S. (2003) *Trends Cell Biol.* **13**, 447–451.
32. Hua, W., Chung, J. & Gelles, J. (2002) *Science* **295**, 844–848.
33. Sack, S., Müller, A., Marx, M., Thormählen, M., Mandelkow, E.-M., Brady, S. T. & Mandelkow, E. (1997) *Biochemistry* **36**, 16155–16165.
34. Nogales, E., Wolf, S. G. & Downing, K. H. (1998) *Nature* **391**, 199–203.
35. Jones, T. A., Zou, J. Y., Cowan, S. W. & Kjeldgaard, M. (1991) *Acta Crystallogr. A* **47**, 110–119.